11246–11260 *Nucleic Acids Research, 2014, Vol. 42, No. 17* *Published online 02 September 2014*
doi: 10.1093/nar/gku795

Yeast mitochondrial RNAP conformational changes are regulated by interactions with the mitochondrial transcription factor

Srdja Drakulic[1], Liping Wang[2], Jorge Cuéllar[1], Qing Guo[2], Gilberto Velázquez[2], Jaime Martín-Benito[1], Rui Sousa[2,*] and José M. Valpuesta[1,*]

[1]Department for Macromolecular Structures, Centro Nacional de Biotecnología (CNB-CSIC), Madrid 28049, Spain and [2]Department of Biochemistry, University of Texas Health Science Center, San Antonio, Texas, TX 78229-3900, USA

Received May 15, 2014; Revised August 3, 2014; Accepted August 25, 2014

ABSTRACT

Mitochondrial RNA polymerases (MtRNAPs) are members of the single-subunit RNAP family, the most well-characterized member being the RNAP from T7 bacteriophage. MtRNAPs are, however, functionally distinct in that they depend on one or more transcription factors to recognize and open the promoter and initiate transcription, while the phage RNAPs are capable of performing these tasks alone. Since the transcriptional mechanisms that are conserved in phage and mitochondrial RNAPs have been so effectively characterized in the phage enzymes, outstanding structure-mechanism questions concern those aspects that are distinct in the MtRNAPs, particularly the role of the mitochondrial transcription factor(s). To address these questions we have used both negative staining and cryo-EM to generate three-dimensional reconstructions of yeast MtRNAP initiation complexes with and without the mitochondrial transcription factor (MTF1), and of the elongation complex. Together with biochemical experiments, these data indicate that MTF1 uses multiple mechanisms to drive promoter opening, and that its interactions with the MtRNAP regulate the conformational changes undergone by the latter enzyme as it traverses the template strand.

INTRODUCTION

The single subunit RNA polymerases (RNAPs) form a widespread family of enzymes that represents a subset of the even larger pol A superfamily of nucleic acid polymerases (1–3). The first recognized member of this superfamily was DNA Pol I from *Escherichia coli*, and the best characterized member of the single-subunit RNAPs is that from bacteriophage T7. In addition to forming part of the genomes of many phages, single-subunit RNAP homologues are encoded in all eukaryotic nuclear genomes and are functionally expressed in chloroplasts and mitochondria, where they transcribe these organelles' messenger and ribosomal RNAs, and also prime replication of their genomes (1,2,4,5).

Comparison of the primary and tertiary structures of the single-subunit RNAPs reveals that they all display an architecture common to the broader pol A superfamily (3). All of these enzymes conserve a polymerase domain that contains the catalytic site and the template binding cleft, which is shaped like a cupped right hand with thumb, palm and fingers subdomains. Different members of this family also exhibit structurally distinct domains, N-terminal to the polymerase domain, which are responsible for distinct functions of different family members. DNAP I, e.g. contains an N-terminal exonucleoytic proofreading domain (6), while T7 RNAP displays an N-terminal domain (NTD) that participates in sequence-specific promoter interaction and binding of the nascent RNA (7,8). The recently described structure of the human mitochondrial RNAP (MtRNAP) repeats this pattern, as it resembles a T7 RNAP molecule to which is appended, at its N-terminus, a ∼370-residue N-terminal extension domain that is structurally unrelated to any elements that have been described in the phage enzymes (9).

The eukaryotic organellar RNAPs are properly described as single-subunit enzymes, since all catalytic activities reside in a single polypeptide which carries out processive, template-directed RNA chain extension without the need for any accessory proteins. However, the mitochondrial

*To whom correspondence should be addressed. Tel: +34 915 854 690; Fax: +34 915 854 506; Email: jmv@cnb.csic.es
Correspondence may also be addressed to Rui Sousa. Tel: +1 210 567 8782; Fax: +1 210 567 8778; Email: sousa@biochem.uthscsa.edu
Present Address: Srdja Drakulic, Department for Molecular Microbiology and Infection Biology, Centro de Investigaciones Biológicas (CIB-CSIC), Madrid 28040, Spain.

RNAPs are functionally distinct from the phage enzymes in that they require one or more transcription factors to open the promoter and initiate transcription, though these factors are dispensable during transcript elongation (10,11). Because fundamental structure-mechanism relationships in the phage RNAPs have been so effectively characterized, the most important questions for the MtRNAPs concern those aspects of structure and mechanism that are distinct from the phage polymerases. In particular, how does the initiation factor(s) function in the transcription cycle? To address this we have used both negative staining and cryo-electron microscopy (cryo-EM) to generate three-dimensional (3D) reconstructions of yeast MtRNAP:promoter complexes (quasi-ICs); initiation complexes (ICs) comprised of promoter, MtRNAP and the yeast mitochondrial transcription factor (MTF1), and elongation complexes comprised of MtRNAP, RNA and DNA. Together with biochemical data these 3D reconstructions reveal that the transcription factor drives promoter melting through multiple mechanisms and that, while the MtRNAP goes through a conformational cycle during transcription that bears similarity to that seen in the phage RNAPs and other pol A enzymes, the MtRNAP conformational cycle is distinct in that it is regulated by interactions with the transcription factor.

MATERIALS AND METHODS

Enzyme and template preparations

MTF1 and MtRNAP mutants were constructed with the Stratagene polymerase chain reaction site directed mutagenesis kit following manufacturer's instructions. Expression and purification of mutant polymerases and MTF1 transcription factor were carried out as described (10), except that proteins were expressed by growing cells to OD of 0.4 at 37°C, following which cultures were transferred to 16°C for 30 min, at which point isopropyl β-D-1-thiogalactopyranoside (IPTG) was added to induce expression and the cultures were incubated for a further 24–48 h at 16°C. Purified proteins were stored at −20°C in buffer containing 10 mM Tris–HCl pH 8.0, 0.5 M NaCl, 1 mM ethylenediaminetetraacetic acid (EDTA), 5 mM dithiothreitol (DTT) and 50% glycerol. DNAs or RNAs were synthesized by Integrated DNA Technologies, dissolved at 1 mM concentration in 20 mM Tris pH 8.0, 50 mM NaCl, 1 mM EDTA, and subsequently annealed by mixing with equimolar amounts of complementary oligonucleotides in the same buffer, heating to 95°C for 5 min, and slow cooling for 2 h at room temperature before being stored at −20°C. Complexes for EM analysis were prepared by mixing equimolar amounts of yeast MtRNAP and annealed templates (with or without equimolar MTF1) followed by dialysis for 12–16 h at 4°C into 10 mM Tris–HCl pH 8.0, 50 mM NaCl, 1 mM EDTA, 2 mM DTT and 50% glycerol with final concentration of complexes of 10 μM. Streptavidin labeled complexes were prepared by subsequently adding streptavidin (Sigma-Aldrich) at 3-fold molar excess (to limit binding of multiple complexes to the tetrameric streptavidin) to complexes which had been assembled from DNAs synthesized with biotin at the 5′-ends. To assess complex homogeneity, as well as to compare complex stability on different promoter templates in competition experiments, native polyacrylamide gel electrophoresis (PAGE) was used. Four microlitre of the assembled complexes were electrophoresed on 8–25% polyacrylamide gels with native buffer strips on a Pharmacia PhastSystem electrophoresis apparatus. Complexes were visualized by staining with coomassie blue or with a Molecular Dynamics Storm Imager with complexes assembled with DNAs labeled at their 5′-ends with fluorescein.

Transcription assays

In vitro transcription reactions were carried out at room temperature for 30 min in 10 μl in transcription buffer (50 mM Tris–HCl (pH 8.0), 10 mM NaCl, 20 mM $MgCl_2$, 10 mM DTT) and nucleoside triphosphates (NTPs) at concentrations indicated in individual figure legends and 0.2 μM template. RNA synthesis was initiated by addition of 0.4 μM yMtRNAP and 0.8 μM MTF1. Transcripts were labeled by inclusion of 1% (v/v) 3000 ci/mM 10 mCi/ml [α-33 P] adenosine triphosphate (ATP) from ICN. Reaction samples taken at the time points specified in individual figure legends were quenched by addition of an equal volume of stop buffer (95% formamide, 20 mM EDTA, 0.01% xylene cyanol). Transcription products were resolved by electrophoresis in 20% (w/v) polyacrylamide gels (19% acrylamide, 1% bis-acrylamide, 7 M urea) in Tris/Borate/EDTA (TBE) buffer and analyzed with a Molecular Dynamics Phosphorimager.

Carboxypeptidase Y sensitivity

The sensitivity of MTF1 to carboxypeptidase digestion was assessed in experiments with 10 μM MTF1 with or without promoter DNA or MtRNAP in transcription buffer (minus DTT) with 0.01 μ/ml of carboxypeptidase Y. Reaction aliquots at different times were taken and stopped by adding 1% v/v of a 100 mM PMSF solution in isopropanol. Digests were analyzed by denaturing (sodium dodecyl sulphate) PAGE on 10% polyacrylamide/bis-acrylamide gels. The band corresponding to MTF1 was excised and analyzed by mass spectrometry.

DNA cleavage with Fe-BABE conjugated proteins

For Iron (S)-1-p-bromoacetamidobenzyl EDTA (Fe-BABE) cleavage experiments the 5′-end of the template (T) or non-template (NT) strands of the DNAs were labeled with [γ-32P]ATP (4000 Ci/mmol; ICN) with T4 polynucleotide kinase (Invitrogen) as described (12). Fe-BABE (Dojindo Laboratories) was conjugated to cysteine substituted MTF1 or MtRNAPs as described (13). ICs halted at +0, +3 or +7, were formed at room temperature in transcription buffer containing labeled bubble or duplex yeast 14 s rRNA promoter template at 0.01 μM, MtRNAP at 0.03 μM and MTF1 at 0.06 μM. After a 10 min incubation with varying NTP mixes to form complexes halted at different positions, cleavage was initiated by addition of sodium ascorbate and H_2O_2 as described (14). Cleavage reactions were quenched after 5 s by addition of one reaction volume of stop buffer (95% formamide,

20 mM EDTA, 0.1% xylene cyanol). Cleavage products were analyzed by electrophoresis in denaturing 15% polyacrylamide gels (14.2% acrylamide, 0.8% bisacrylamide and 7 M urea) and visualized on a Molecular Dynamics Pphosphorimager. Cleavage positions were mapped by reference to Maxam–Gilbert G + A ladder prepared as described (15).

Electron microscopy and image processing

Aliquots of the different transcription complexes (quasi-IC, upstream labeled quasi-IC, IC, upstream and downstream-labeled IC, EC, upstream and downstream labeled EC, spRNAPIV elongation complex (EC) and downstream labeled spRNAPIV EC) were applied onto previously glow-discharged carbon-coated copper/rhodium grids and stained with 2% uranyl acetate. Images were recorded under minimal-dose conditions on Kodak SO-163 film, in a JEOL JEM1200EXII microscope operated at 100 kV and 60 000 magnification. Micrographs were digitized using a ZEISS scanner with the step size of 14 μm, resulting in a pixel size of 2.33Å.

For cryoEM, aliquots of IC and EC were applied onto glow-discharged, holey carbon grids (carbon-coated Quantifoil R 1.2/ R1.3 300 mesh grids) containing an additional continuous thin layer of carbon, and plunged into liquid ethane. Images were acquired under minimal dose conditions with a Tecnai F20 transmission electron microscope at 200 kV. The images were taken at magnification of ∼110 000 using a 16 megapixel (Mpx) FEI Eagle CCD camera with a step size of 15 μm, thus the original pixel size of the acquired images was 1.37 Å. Cryo-EM micrographs were downsampled by a factor of 2 or 3 (EC and IC, respectively). The contrast transfer function of the each acquired image was estimated using CTFFIND3 program (16) and corrected at the micrograph level. Individual particles were selected manually and extracted using XMIPP software (17) (Supplementary Figure S2A). Two types of free-pattern maximum-likelihood multi-reference refinement approaches ('Maximum Likelihood 2D' (ML2D) (18) (Supplementary Figure S2B) and 'Clustering 2D' (CL2D) (19)) were carried out with normalized particles. Homogeneous populations were obtained and averaged for a final two-dimensional (2D) characterization.

Several starting reference models and initial 3D reconstruction steps based on iterative angular refinement were performed using the EMAN software package (20). In general the initial volumes were created upon the class averages generated in the previous step, using a common lines approach or by using artificial noisy models and Gaussian blobs with the rough dimensions of the protein complexes. In the case of the streptavidin labeled complexes and those complexes analyzed by cryo-EM, the previously obtained EM maps of non-labeled or negatively-stained complexes were filtered to 70 Å, and used as the initial models. The different strategies converged to similar solutions, and one of the models was selected to complete the refinement (Supplementary Figure S2C). However, in the case of heterogeneity (EC cryo-EM; streptavidin-biotin labeled ICs) the most stable model was subjected to maximum likelihood 3D classification (ML3D) (18) to address this problem. The separated particles were processed using EMAN and the whole 3D reconstruction cycle was repeated *de novo*. The resolution of the reconstructions was determined by the FSC 0.5 criterion (Supplementary Figure S3), and these values were used to low-pass filter the final volumes. The visualization of density maps and atomic structures was performed using UCSF Chimera (21). The dockings were firstly performed manually and then rendered by Chimera, using a real time correlation criterion between the reference model (final model) and the surface created from the atomic structure/model. The final validation of the obtained models was performed by comparison of the final 3D map projections and the generated class averages (EMAN) with the results of 2D classifications (Supplementary Figure S2B).

RESULTS

Structural characterization of yeast MtRNAP IC without MTF1 ('quasi IC')

Formation of the yeast mitochondrial initiation complex (IC) requires yeast MtRNAP (1324 residues) and MTF1 (341 residues) which, together, form a stable complex with a duplex mitochondrial promoter DNA (11,22). A stable complex can also be assembled between the MtRNAP alone and a 'pre-melted' promoter (Supplementary Figures S1A–C; bubble promoter or 'IC DNA') bearing sequence changes in the NT strand to create a mismatched +2 to −4 region (10). Because we wanted to identify MTF1 and MtRNAP in the 3D reconstruction of the IC, we sought to image ICs formed without MTF1 (quasi-ICs) as well as true ICs formed with both proteins. It is, however, possible that complexes formed on the pre-melted promoters do not genuinely recapitulate the structures of complexes formed on fully duplex promoters. We therefore used chemical nucleases tethered to cysteines introduced into MTF1 or MtRNAP to compare the structure of ICs formed on duplex versus pre-melted promoters. We observed that these nucleases cut the promoter DNA at nearly identical locations on both types of promoters, and that, upon addition of NTPs that allowed extension of the RNA to different lengths, these cleavage sites shifted identically on both the fully duplex and pre-melted promoters (Supplementary Figures S1D and E). The ICs formed on the pre-melted and duplex promoters are therefore structurally and functionally similar.

A total of 12848 images of negatively stained particles formed with the MtRNAP and a 29 bp promoter DNA in which the −2 to +4 region was heteroduplex were used to generate a 3D reconstruction of a quasi-IC (Figure 1A and B; see also Supplementary Figures S2 and S3A), revealing a compact structure. The pol A class polymerases display a polymerase domain with the shape of a cupped right hand that forms a cleft in which the DNA binds. This central cleft is apparent in the 3D reconstruction of the quasi-IC, but is narrower than typically seen in other pol-A class polymerases (Figure 1C). The narrowness of this cleft in the quasi-IC seems to correspond to the 'clenched' conformation with a constricted central binding cleft observed in human MtRNAP (23) (Figure 1A), and this notion is strengthened by a better docking correlation value with this atomic structure (PDB ID: 3SPA; 0.85) than with that of

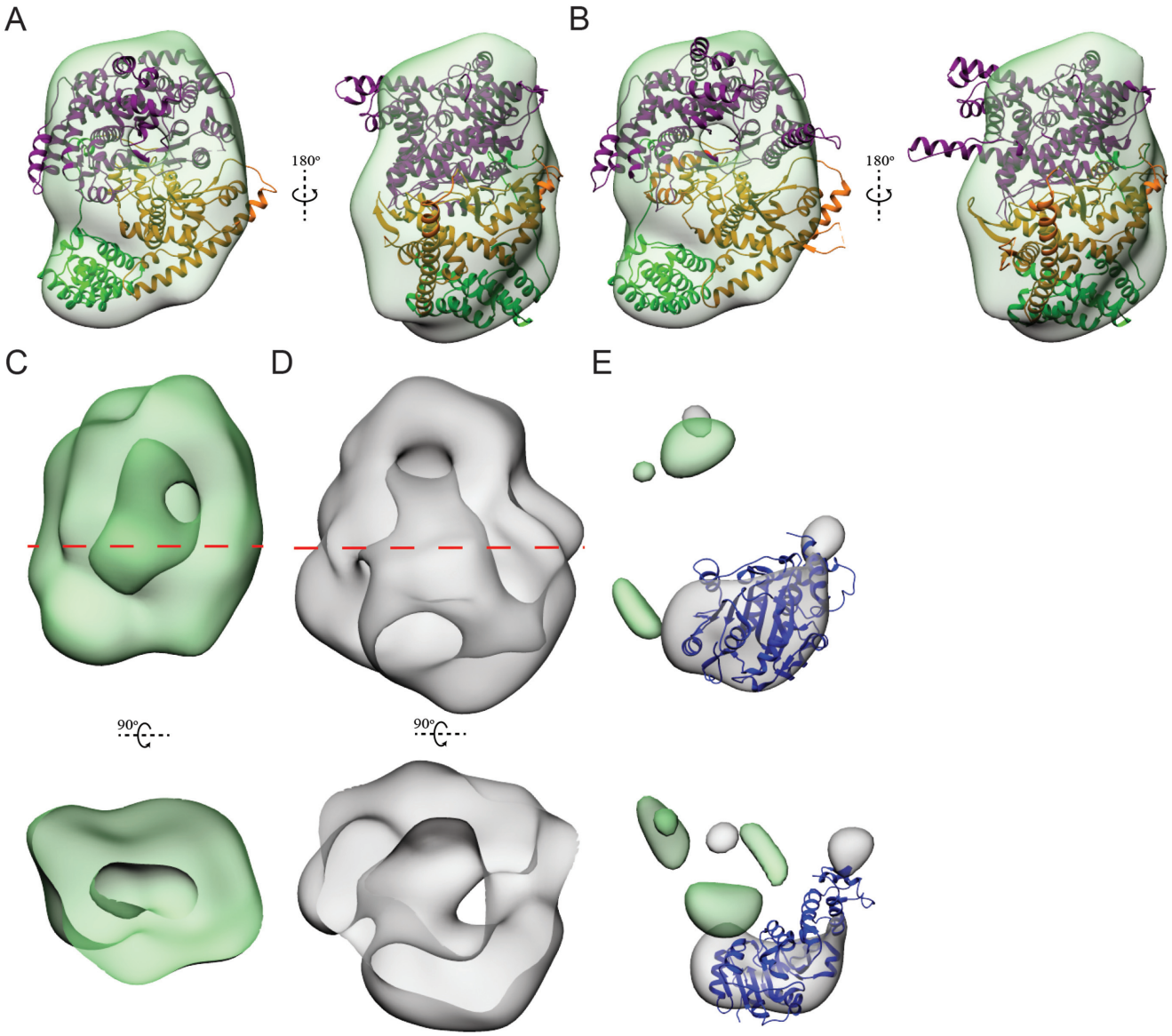

Figure 1. A yeast MtRNAP quasi-IC assumes a clenched conformation while the IC assumes an open state. (**A**) The 19 Å resolution yeast MtRNAP quasi-IC structure reconstructed from 12848 negatively stained particles assembled from MtRNAP and a 29 bp pre-melted promoter DNA. Docked into the 3D reconstruction is the atomic structure of DNA-free human MtRNAP (PDB ID: 3SPA (23)) with residues 218–383 (N-terminal extension domain) in green, residues 384–672 (the N-terminal domain or NTD) in orange and residues 673–1230 (C-terminal, polymerase, catalytic domain) in purple. (**B**) As in (A), but with the atomic structure of human MtRNAP EC (PDB ID: 4BOC (24)) docked in; the DNA is not shown) (**C**) The quasi-IC 3D reconstruction rotated as indicated and cut at the plane indicated by the red line. (**D**) The IC reconstruction rotated as indicated and cut at the plane indicated by the red line (**E**) Difference map (gray volumes) generated by subtracting the IC from the quasi-IC with the atomic structure of MTF1 (PDB ID: 1I4W; blue) placed on the large density difference.

mtRNAP EC (PDB ID: 4BOC; 0.84) (Figure 1B), but specially by a 3D reconstruction of quasi-IC with DNA labeled with streptavidin at its upstream end ('upstream streptavidin quasi-IC'), generated from 16514 particles (Supplementary Figure S3B; 18 Å resolution) in which the streptavidin molecule (and therefore the 5′-end of the NT-strand DNA) is located closer to the polymerase domain. These results point to the yeast MtRNAP in quasi-IC having a clenched conformation

Yeast MtRNAP IC with MTF1 assumes an open conformation

To compare the quasi-IC conformation to that of a true IC, we carried out a 3D reconstruction of the IC at 22 Å resolution (Figures 1D, 2A and Supplementary Figure S3D) using 15917 negatively stained particles formed with yeast MtRNAP, MTF1 and the 29 bp pre-melted promoter DNA (Supplementary Figure S1B). Both our native gels and inspection of EM fields of negatively-stained quasi-ICs and ICs indicated that the quasi-IC had a tendency to oligomerize that was suppressed in the IC. The excep-

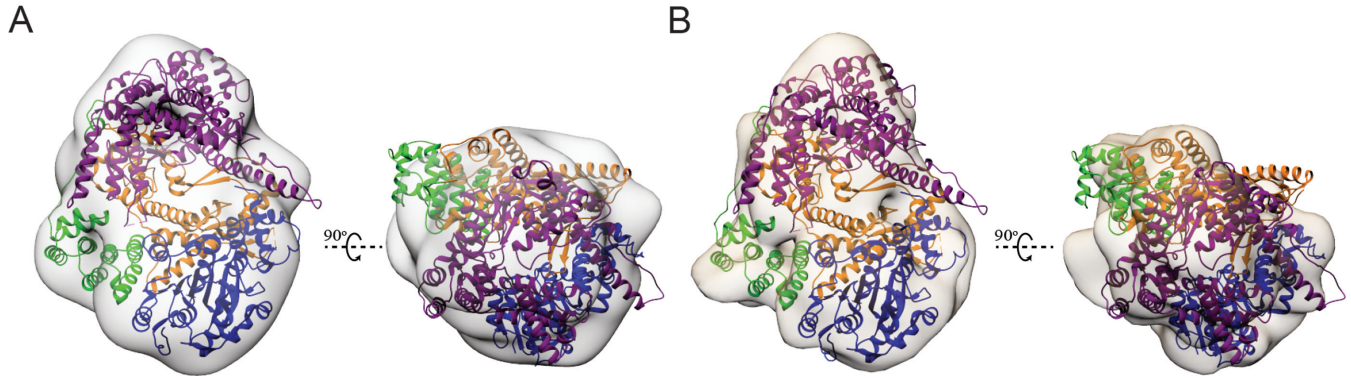

Figure 2. Positioning MTF1 in the IC. (**A**) Two orthogonal views of the 3D reconstruction of yeast MtRNAP IC with MTF1 (blue) and the atomic structure of yeast MtRNAP (modeled on the human MtRNAP structure) fit into the reconstruction. The yeast MtRNAP N-terminal extension (residues 240–383), NTD (residues (384–672) and the polymerase domain (residues 673–1233; 1317–1351) are in green, orange and purple, respectively, while the atomic structure of MTF1 is in blue. (**B**) The same two views of the 3D reconstruction of yeast MtRNAP IC with MTF1 generated from unstained, frozen particles. Docking as in (A).

tional homogeneity of the IC particles and their relatively large size (∼210 kDa) prompted us to attempt an EM reconstruction of the IC by cryo-EM. A total of 10 893 particles were used to generate a 15 Å resolution 3D reconstruction of the IC (Figure 2B and Supplementary Figure S3C). Comparison of the IC reconstructions obtained by negative staining and cryo-EM show them to be very similar (compare Figure 2A and B; see also Supplementary Figure S3C and D). We therefore aligned these two reconstructions and both docked well with the atomic structure of human MtRNAPEC (the correlation coefficient values were 0.84 and 0.81 for the docking into the EM structures originating from frozen and negatively stained samples, respectively). In human MtRNAP, the transition from the clenched, DNA-free to the open, elongation state involves the rotation of the palm and fingers domains by 10° and 15°, respectively. The resulting conformation of human MtRNAP in EC resembles to that of the intermediate IC of T7 RNAP, the state with a 7 nts long RNA (24). Thus, we suggest that the conformation of MtRNAP in the IC is closer to the EC than to the clenched form found in the quasi-IC. Indeed, the IC as a whole, and the central, template-binding cleft, were found to be wider than in the quasi-IC (compare the cavities in the structures shown in Figure 1C and D).

Localization of MTF1 in the IC

The shape of the largest density element in the difference map obtained by subtraction of the IC from the quasi-IC is similar to the atomic structure of MTF1 (Figure 1E). MTF1 is a dumbbell-shaped molecule comprised of a larger mixed helical/sheet NTD and a smaller, helical C-terminal domain (25). Overall, the molecule has concave and convex sides that, together with the differences in the sizes of the two lobes of the dumbbell, allow us to orient the MTF1 with the C-terminal domain at the narrower end of the difference density and with the concave side facing the MtRNAP (Figures 1E and 2). This positions MTF1 in the IC with its concave and more electropositive side facing the electropositive surface of the MtRNAP which forms the DNA and RNA binding sites of the polymerase (Figures 2 and 3; see also Supplementary Figures S3C and D). The two 3D reconstructions therefore indicate that MTF1 binds the IC so as to sandwich the DNA between the electropositive surfaces of the polymerase and the transcription factor.

Localization of DNA in the IC

To better reveal how the DNA binds in these complexes we carried out 3D reconstructions of negatively stained ICs formed with DNAs in which either the upstream (5′-NT strand end) or downstream (5′-T strand end) segments were labeled with biotin and then reacted with streptavidin. The 3D reconstruction of the IC with streptavidin labeling the upstream end of DNA ('upstream streptavidin IC') reveals an extra density, appropriate for accommodating the streptavidin molecule, connected to the NTD of the MtRNAP by a tube of density (Supplementary Figure S3F). Interestingly, the position of the streptavidin matches the position of the upstream DNA termini of the aligned 3E2E atomic structure, the structure of T7RNAP IC with a 7 nts long RNA (Figure 4B). Furthermore, this part of the DNA is located near the positively charged cleft and at the end of the C-terminal domain (C-terminal tail) of MTF1, the MtRNAP's C-terminal domain, the AT-rich recognition loop and intercalating β hairpin, which as seen in the T7RNAP IC, inserts between the T and NT strands at the upstream edge of the transcription bubble (26,27). To identify the downstream segment of the DNA we generated a 3D reconstruction of an IC in which the downstream DNA end was labeled with streptavidin bound to biotin linked to the 5′-end of the T strand ('downstream streptavidin IC'), revealing an extra density that is not occupied by the atomic model of the IC (Supplementary Figure S3E). This density is appropriate in size and shape to accommodate the 50 kDa streptavidin tetramer, and sits adjacent to the N-terminal extension (Figure 4A). The position of the downstream end of DNA in 3E2E clashes with the NTD of MTF1, which suggests its placement deeper in the extended binding cleft formed by the MtRNAP and MTF1, also indicating it to be less accessible to streptavidin binding. Thus, the positions of upstream and downstream termini of DNA in the yeast

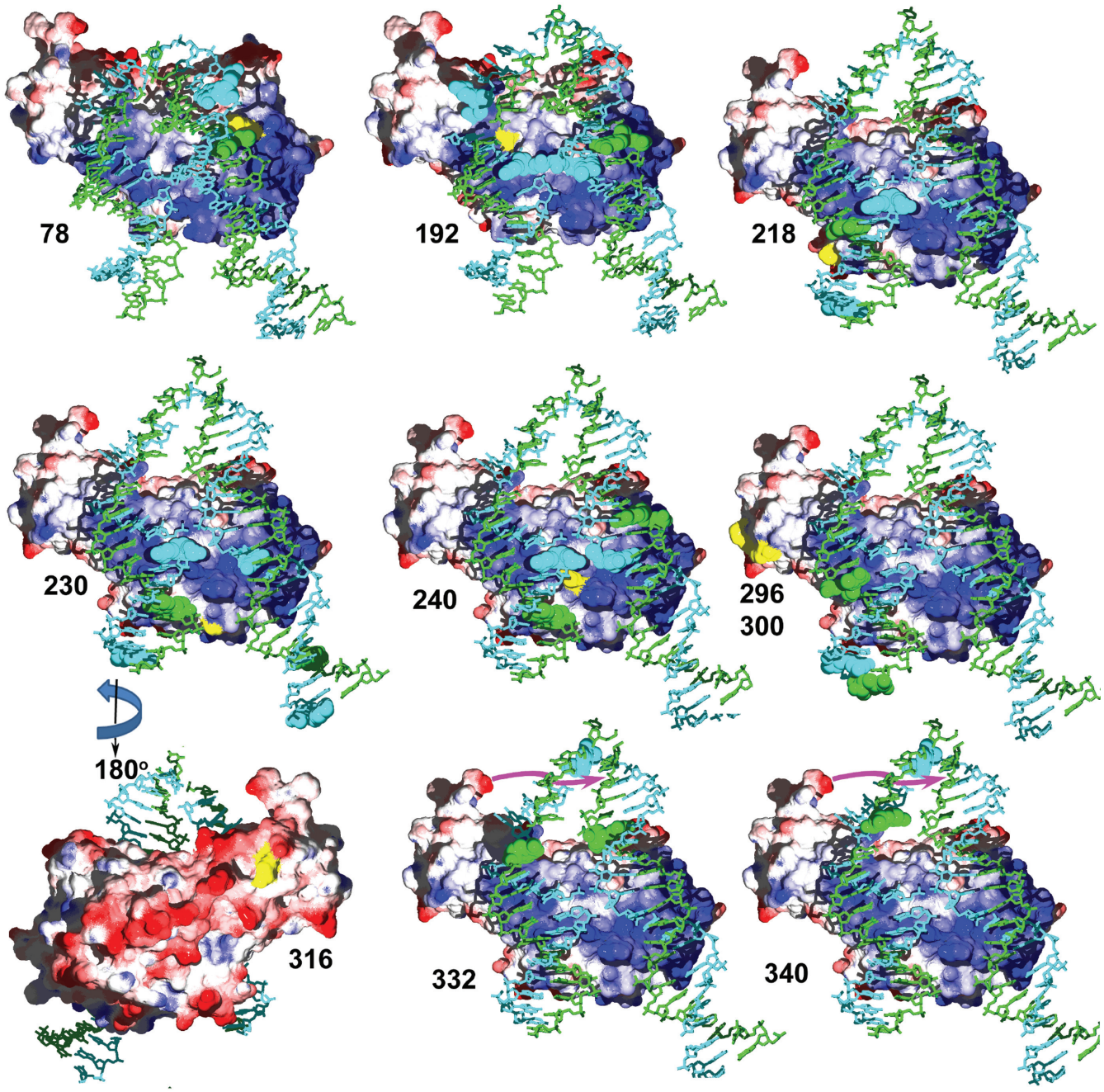

Figure 3. Localization of Fe-BABE cleavage sites on MTF1:IC–DNA models. Each panel shows the MTF1 structure (25) in surface representation with −, + and uncharged regions in red, blue and white, respectively. The DNA is in stick representation with the T-strand in cyan and the NT-strand in green. The DNA is placed on MTF1 as proposed in our IC model based on steric considerations, EM data, the positions of the intercalating hairpin (stacked on the −4 bp) and active site aspartates (nearest the T-strand +2 ribose), and the positions of the sites cut by Fe-BABE conjugated to different sites on MTF1. In each panel the position of the residue(s) to which Fe-BABE was conjugated is labeled and highlighted in yellow, and the centers of the sites of cleavage by those conjugates are indicated by showing the corresponding DNA nucleotides in space-filling representation. For the conjugates to residues 332 and 340 , which correspond to residues on the disordered C-terminal tail of MTF1, the magenta arrow shows the possible position of the C-terminal tail based on the observation that conjugates to either of these residues cut within the unwound region of the promoter.

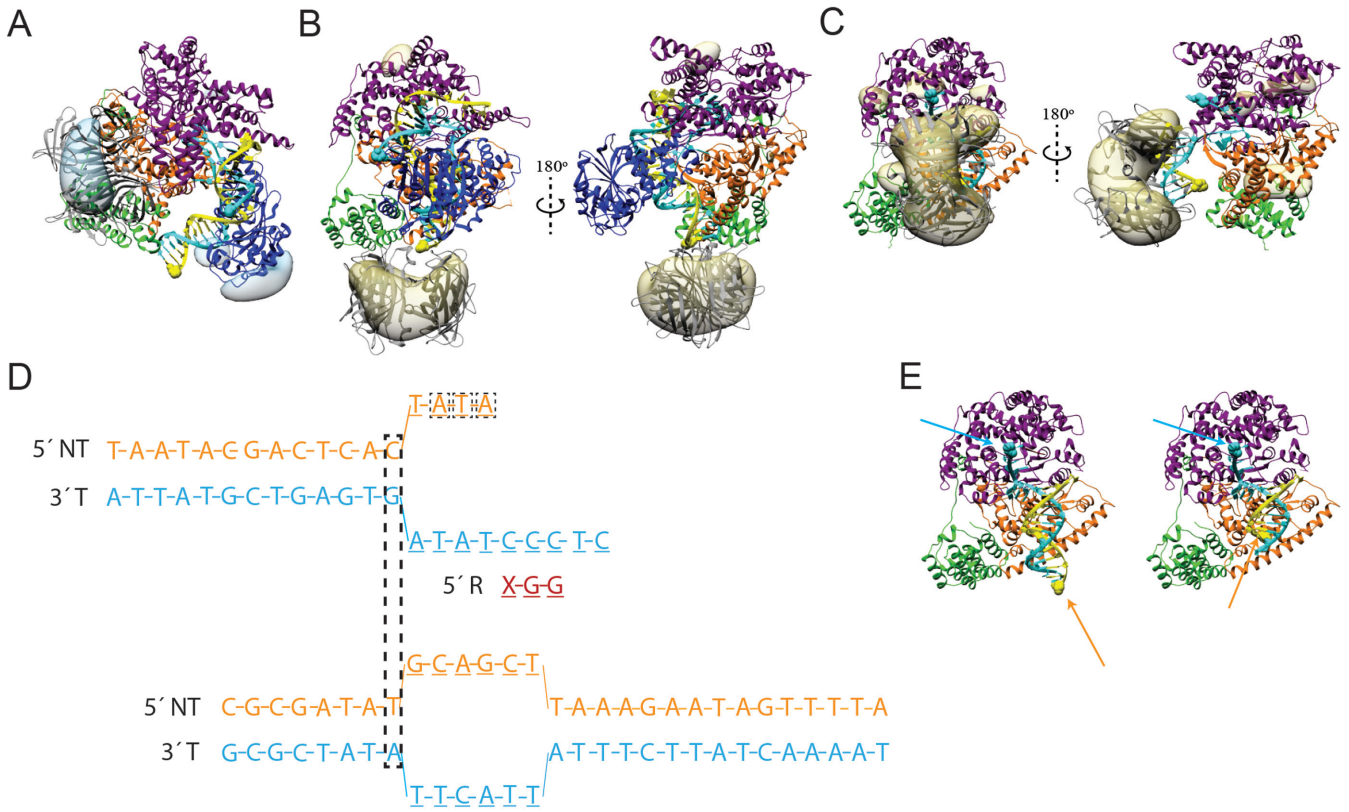

Figure 4. Localization of DNA in the IC. (**A**) Difference map (light blue volumes) generated by subtracting the IC from the downstream streptavidin IC with the atomic structure of streptavidin (PDB ID : 1N43: gray) placed on the large density difference. The atomic structure of T7RNAP in the 7 nts RNA long IC state (PDB ID : 3E2E) has been aligned with the previously fitted atomic structure of human MtRNAPEC. The 3E2E DNA molecule (NT strand dyed in yellow and T strand in cyan) is shown, with downstream and upstream ends emphasized by blue and yellow spheres. (**B**) Two views of the difference map (yellow volume) generated by subtracting the IC from upstream streptavidin IC. The position of the upstream 3E2E DNA's end is located within the reach of the streptavidin molecule (**C**) Two views of the difference map (gray volume) generated by subtracting the upstream streptavidin quasi-IC from quasi-IC. The docked atomic structure of human MtRNAP (PDB ID: 3SPA) is shown together with the DNA of aligned atomic structure of T7RNAP at 3 nts long RNA IC state (PDB ID: 1QLN). The DNA length has been adjusted according to (**D**). NT and T strands are colored as in (A) and (B), yellow and cyan respectively. (**D**) Schematic representation of DNA sequence of 3E2E, top and of one used in this study, bottom, to form quasi-IC and IC. The boxed ATA sequence of NT-strand is not visible in the 3E2E atomic structure. The upstream edges of transcription bubbles are taken as a reference point for the alignment, allowing the adjustment of 3E2E DNA's length according to the length of the DNA used in this study. (**E**) Docked atomic structure of PDB ID: 3SPA shown with the original aligned 3E2E DNA (left) and adjusted DNA (right).

IC are close to their position in the T7RNAP IC with a 7 nts long RNA (the late IC). This, together with the structural resemblance of these polymerases strongly suggests that yeast MtRNAP in complex with MTF1 acquires a conformation similar to the T7RNAP late IC.

This raises a question of how the quasi-IC, with its narrower cleft, binds DNA. When the 3D reconstructions of quasi-IC and IC, both with DNA labeled with streptavidin at their upstream end are compared (Supplementary Figure S3B and F, respectively), it can be observed that the streptavidin in the quasi-IC is located closer to the polymerase domain than in IC (compare Figure 4B and C). Thus, binding of MTF1 is associated with an increased bending of the DNA in the complex and binding of the upstream segment of the promoter toward regions on the MtRNAP NTD(s), consistent with previously reported differential bending of promoter DNA by yeast MtRNAP alone versus the yeast MtRNAP:MTF1 complex (28). A similar change in DNA bending is observed in T7RNAP in the initiation steps of transcription—upon the incorporation of the 7th nucleotide to the nascent RNA molecule, the N-terminal part of the enzyme (residues 72–152 and 191–267) and the specificity loop are rotated ∼45° (29). This rigid body rotation does not affect the contacts with the promoter, causing its additional bending. We have aligned the atomic structure of the T7RNAP IC with a 3 nts RNA (PDB ID: 1QLN (30) with the docked atomic structure of human MtRNAP. If the upstream edges of transcription bubbles are taken as a reference point (since the intercalating β hairpins which insert at the upstream edge of the transcription bubble play similar roles in T7RNAP and yeast MtRNAP transcription initiation (27)), then the upstream end of the IC DNA used in this study can be modeled on the DNA of 1QLN (Figure 4D and E). The modeled position is in the range of the upstream streptavidin molecule that represents the experimentally defined position of the upstream DNA terminus (compare Figure 4C and E). The conformation of T7RNAP without the DNA and with the DNA and 3 nts long RNA, is similar. However, the specificity loop and β-intercalating hairpin become structured upon DNA bind-

ing. The same can be observed for these elements when the DNA-free and DNA-bound structures of human MtRNAP are compared. This, together with the position of the upstream end of the DNA in the quasi-IC, which matches that in the T7RNAP IC with 3 nts RNA, suggest that, in the absence of MTF1, DNA-free and DNA-bound MtRNAP assume a similar conformation.

Chemical nucleases tethered to MTF1 inform IC modeling

To test and refine our structural model of IC generated from the EM images of the quasi-IC and IC, and of the streptavidin-labeled complexes, we used the chemical nuclease p-bromoacetamidobenzyl ethylenediaminetetraacetate (Fe-BABE (31)) conjugated to MTF1 cysteines. Upon reaction with peroxide, Fe-BABE generates a local burst of diffusible hydroxyl radicals that cut nearby DNA strands, with the intensity of cutting determined by distance and accessibility. MTF1 conjugated with Fe-BABE cut both T and NT DNA strands in an IC (Supplementary Figure S4B). To determine which of the various MTF1 cysteines was conjugated with the Fe-BABE that was generating these cuts, we individually mutated each of the two surface exposed cysteines on the DNA-binding face of MTF1 (C69 and C192) to serines (mutation of buried cysteine residues caused MTF1 to aggregate during expression. There are two other surface exposed cysteines in MTF1: C220 and C320. C220 is on the side the opposite to that which is identified as binding DNA, while C320 is within the C-terminal tail of MTF1 that is disordered in the crystal structure of MTF1 alone). Mutation of C69 did not affect cleavage patterns (not shown), but the C192S mutation almost completely eliminated the cleavage observed with the wild-type protein (Supplementary Figure S4A and B), indicating that cutting was due to Fe-BABE conjugated to C192 (a C192F mutation has been reported to compromise MTF1 function but we found that a C192S mutant had WT activity (Supplementary Figure S4I–M), suggesting that the isosteric serine substitution is less disruptive of MTF1 activity than the phenylalanine substitution).

We then generated nine other individual cysteine substitutions in the C69S/C192S mutant MTF1 background, expressed and purified these mutants, and conjugated them with Fe-BABE. All of the mutants were in surface exposed residues and were found to be similar in activity to the WT protein (Supplementary Figure S4I). ICs were formed with these Fe-BABE conjugated MTF1 mutants on a 63 bp DNA containing the active 14 s mitochondrial promoter with base changes introduced into the −4 to +2 region of the NT strand to create a heteroduplex region to enhance IC stability (cutting patterns on fully duplex promoters were modestly weaker but otherwise similar to those on the bubble promoter; Supplementary Figures S1B and S4A–H). The DNA in the ICs was labeled at the 5′-end of either the T or NT strand with 33P and cutting was activated by adding peroxide to open complexes (no NTPs), or complexes in which NTPs allowing RNA extension to three or seven nucleotides were present. The data set of all these cutting patterns is presented in Supplementary Figures S4A–H, and is summarized in Figure 3.

The cleavage patterns of the conjugated MTF1 proteins were consistent with the model suggested by the EM 3D reconstructions, MTF1 was placed in the IC so that the duplex down- and upstream segments of the DNA were near the positively charged surface of the NTD and the positively charged region at the border of the N- and C-terminal domains, respectively (Figure 3). The most N-terminal conjugate was at residue 78 and cleaved DNA only at positions downstream of the transcription bubble (Supplementary Figure S4A), while the most C-terminal conjugates within the C-terminal domain (at position 296 and 300) only cut DNA upstream of the unwound region (Supplementary Figure S4F). Conjugates at intermediate positions (192/230/240) cut both up- and downstream DNA (Supplementary Figures S4B, D and E), consistent with the DNA being sharply bent in the IC so that both up- and downstream DNA segments were accessible to hydroxyl radicals generated at these residues. The finer scale features of these cutting patterns also helped to refine the approximate location of MTF1 and DNA in the IC: cutting by conjugates at position 192 was nearest to the apex of the DNA bend (at positions −7/−3/+9/+10, while cutting by the conjugate at 230 was furthest from the unwound region (−17/−11/−8/+12/+18/+21) and the conjugate at 240 cut at intermediate positions (−11/−8/+9/+11). These cutting sites therefore indicated that MTF1 and the DNA should be modeled so that residues 192, 240 and 230 define an axis approximately centered on the apex of the bent DNA and extending parallel to the up- and downstream duplexes, with residue 192 closest to the apex and residue 230 most distant (Figure 3). This placement of MTF1 is consistent with the conclusion that the transcription factor interacts with the unwound NT-strand to favor promoter melting, and with our observations that MTF1 binds quasi-ICs formed with promoters that contain a melted NT-strand more strongly than promoters that are missing the melted NT-strand (Supplementary Figure S4J–M).

Cutting by conjugates attached to residues in the MTF1 C-terminal tail was also informative. The last 16 residues of the MTF1 C-terminal tail, starting from the residue 325, are disordered in the crystal structure of the protein alone (25). Conjugates at residues 332 or 340 within this C-terminal tail cut the NT strand in the IC between −2 and +7, and the T strand between −5 and −2 (Figure 3 and Supplementary Figure S4H). These cuts are either within or immediately up- or downstream of the unwound DNA in the IC and suggest that, upon binding DNA, the C-terminal tail becomes ordered and inserts between the melted DNA strands where it may contribute to promoter opening. Consistent with this, we observed that MTF1 binding to the IC protected its C-terminus from digestion by carboxypetidase (Supplementary Figure S5A).

The MTF1 C-terminal tail contributes to promoter opening

The functional role of the C-terminal tail of MTF1 was then tested by comparing the transcriptional activity and stability of ICs formed with full-length MTF1 or MTF1 with the 17 most C-terminal residues deleted (residues 325–341; corresponding to the disordered region in the MTF1 crystal structure; MTFΔCterm). We observed that on du-

plex promoters, the transcriptional activity in reactions with MTFΔCterm was as high (or higher) than that obtained with full-length MTF1 when the concentration of the initiating NTP (ATP) was high. However, at low initiating NTP concentrations the activity in the MTFΔCterm reactions was markedly reduced compared to those carried out with full-length protein. A similar difference in activity at high versus low ATP concentrations with MTFΔCterm versus full-length MTF1 was not observed on pre-melted promoters (Supplementary Figure S5B and C). Other measurements, including the sensitivity of ICs to varying salt levels and the rates of dinucleotide synthesis as a function of varying ATP concentrations, similarly indicated a specific deficiency in the activity of MTFΔCterm ICs on duplex, but not pre-melted, promoters (Supplementary Figures S5D and E). Fitting of these data showed apparent K_{ATP} to be 4–8-fold greater with MTFΔCterm versus full-length MTF1 on duplex promoters, but identical within experimental error on pre-melted promoters (Table 1).

The structure of the yeast MtRNAP elongation complex (EC)

We undertook a similar set of EM studies of the yeast MtRNAP EC. A synthetic transcription bubble was formed by hybridizing a 10 base RNA to the 5′-segment of a 21 base T-strand annealed to a 21 base NT-strand which was non-complementary to the 10 bases at the 5′-end of the T-strand (Supplementary Figure S1C; 'EC DNA'). Native gel analysis showed that MtRNAP formed a stable complex with this nucleic acid scaffold and extension assays revealed that the RNA was quantitatively extended in a T-strand directed manner by the MtRNAP upon addition of NTPs (Supplementary Figure S1F), confirming that the complexes formed with this scaffold were functional. Both gel analysis and inspection of EM fields revealed that the ECs were highly homogeneous, so we carried out reconstructions of the EC by both cryoEM of unstained, frozen-hydrated particles (9538 particles, 19 Å resolution) and negative staining (20 873 particles, 19 Å resolution). Both 3D reconstructions were very similar (Figure 5A and B; see also Supplementary Figure S6A and B). We also carried out a 3D reconstruction with negatively-stained particles of an EC assembled with an MtRNAP from which residues 1–243 had been deleted, corresponding to a putative nuclear version of the polymerase that has been dubbed spRNAPIV (32). The 3D reconstruction of the spRNAPIV EC was very similar to the negatively stained or cryoEM reconstructions of the full-length MtRNAP ECs (Figure 5C; see also Supplementary Figure S6E), with no additional density apparent in the full-length reconstructions that could be clearly assigned to the element deleted in the spRNAPIV EC (Figure 5A–C). The difference maps obtained by subtracting MtRNAP EC from spRNAPIV EC also failed to show any obvious density that could be assigned to the region deleted in spRNAPIV. Therefore, it is probably that the N-terminal region deleted in spRNAPIV is either wholly or partially disordered and does not contribute to the density in the averaged 3D reconstructions of the full-length MtRNAP. This would be consistent with what is observed with both human MtRNAP structures (PDB IDs: 4BOC (24) and 3SPA (9)), in which residues 1–105 were deleted to enhance crystallization, and in which residues 106–217 are disordered and invisible in the electron density map (23). The atomic structure of human MtRNAPEC (24) fits well into all of the three 3D reconstructions of EC shown here (Figure 5A–C; see also Supplementary Figure S6A,B and E).

Localization of DNA in the EC

The length and sequences of EC DNA scaffolds used in this study and in the atomic structure of human MtRNAPEC (24) are not identical. However, the downstream edge of two transcription bubbles can be used as reference point for alignment, which allows modeling of the position of the EC DNA termini (Figure 5D and E). To confirm this, we carried out 3D reconstructions of negatively stained ECs assembled with nucleic acid scaffolds in which either the upstream or downstream DNA ends were labeled with streptavidin (Supplementary Figure S6C and D and Figure 5F and H). The difference in the positions of both the upstream and downstream DNA termini as modeled from the human MtRNAP EC structure and as experimentally determined by positions of the streptavidin molecules is ∼15 Å (in the case of upstream DNA termini this discrepancy is even smaller as the 5′NT end of DNA used in this study is in the single stranded form, comparing to the corresponding nucleotide at position −10 of DNA in 4BOC). Since the resolution of our structures is in the 15–25 Å range, this represents excellent quantitative agreement between the human MtRNAP EC crystal structure and our EM reconstructions.

Using the positions of the streptavidin molecules to compare the positions of the DNA IC and EC reveals a clear displacement of its upstream end during the transition from the IC to EC (Figure 6A and B). To test this further we conjugated Fe-BABE to cysteines introduced into the MtRNAP C-terminal domain on the thumb (at residue 780) and fingers subdomains (at residues 1025, 1074 and 1078), and on the NTD (at residue 493). The conjugates on the thumb and fingers subdomains cut DNA either within or immediately downstream of the transcription bubble in both the IC and EC, and generally tracked the downstream movement of the RNAP as the RNA was extended (Figure 6C; the conjugate on the thumb also showed discontinuous changes in cutting during initial transcription, as is also seen in similar experiments with T7RNAP (13)). However, the conjugate on the NTD exhibited cutting in ICs, but not the EC, consistent with the observed displacement of the upstream end of DNA

The N-terminal extension domain appears to be involved in formation of the downstream edge of the transcription bubble (33), which led us to ask ourselves if the N-terminal deletion in spRNAPIV might affect DNA binding to EC. To address this, we generated a 3D reconstruction of spRNAPIV and DNA labeled with streptavidin at its downstream end (see Supplementary Figures S6E and F). In the 3D reconstruction of the spRNAPIV EC the streptavidin molecule is located at a similar position as in the downstream labeled version of the full length MtRNAP EC (compare Figure 5F and G), indicating that the deletion does not grossly alter the position of the downstream DNA.

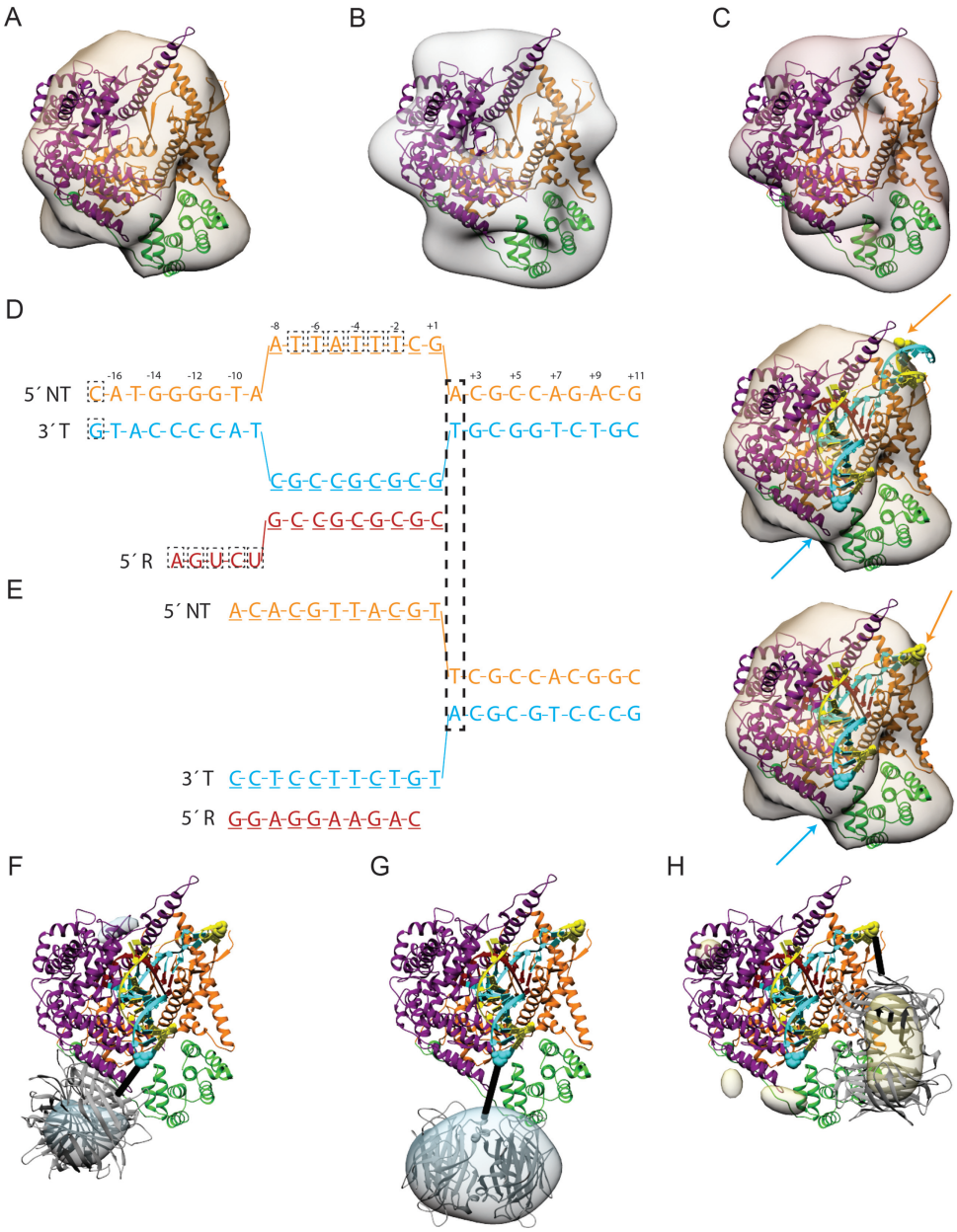

Figure 5. 3D reconstruction of the EC. (**A**) 3D reconstruction of the yeast MtRNAP EC generated from unstained, frozen particles. The atomic structure of human EC (PDB ID: 4BOC (24)) is fitted into the 3D reconstruction (correlation coefficient 0.74). (**B**) As in (A), but for a 3D reconstruction generated from negatively stained particles. The atomic structure of human EC (PDB ID: 4BOC (24)) is fitted into the 3D reconstruction (correlation coefficient 0.84). (**C**) As in (B), but for ECs prepared with an MtRNAP from which the first N-terminal 243 residues were deleted (spRNAPIV EC). The atomic structure of human EC (PDB ID: 4BOC (24)) is fitted into the 3D reconstruction (correlation coefficient 0.92). (**D**) Left: schematic representation of EC DNA scaffold used in (24). Template and non-template strands are dyed in cyan and yellow, respectively. Cyan: 28 nts long non-template strand with nucleotides not visible in X-ray structure indicated by dashed squares; Orange-yellow: 28 nts long template strand with nucleotide not visible in X-ray structure indicated by dashed square; Red: 14nts long RNA. Underlined nucleotides are ones that form a transcription bubble. Right: docking of the human MtRNAPEC (PDB ID: 4BOC) in the cryo-EM map of yeast MtRNAPEC, obtained in this study. Template and non-template strands are dyed in cyan and yellow, respectively. Upstream (5′NT) and downstream (5′T) DNA termini are emphasized with spheres colored in yellow and cyan respectively. (**E**) Left: schematic representation of EC DNA scaffold used in this study, aligned with the DNA presented in (A), using the upstream edge of transcription bubble as a reference, alignment point. 21 nts long template and non-template strands are dyed in orange (yellow) and cyan, respectively, while 10 nts long RNA in red. Underlined nucleotides are ones that form a transcription bubble. Right: docking of the human MtRNAPEC (PDB ID: 4BOC) in the cryo-EM map, obtained in this study. Template and non-template strands are dyed in cyan and yellow, respectively. Positions of the upstream (5′NT) and downstream (5′T) DNA termini, shown with spheres colored in yellow and cyan respectively, are adjusted according to the alignment. (**F**) Difference map in which the 3D reconstruction of negatively stained EC was subtracted from the 3D reconstruction obtained from EC particles in which the downstream DNA end was labeled with streptavidin (‘downstream streptavidin EC’). The scale bar indicates a difference in positions of expected, theoretical (blue spheres) and experimental (streptavidin) downstream end of DNA (5′ terminus of NT strand) (**G**) Difference map in which the 3D reconstruction of negatively stained spRNAPIV EC was subtracted from the 3D reconstruction obtained from spRNAPIV EC particles in which the downstream DNA end was labeled with streptavidin (‘downstream streptavidin spRNAPIV EC’) (**H**) As in (F), but this time the subtraction is performed between the 3D reconstruction of EC and a 3D reconstruction of EC in which the upstream end of the DNA is streptavidin-labeled (‘upstream streptavidin EC’).

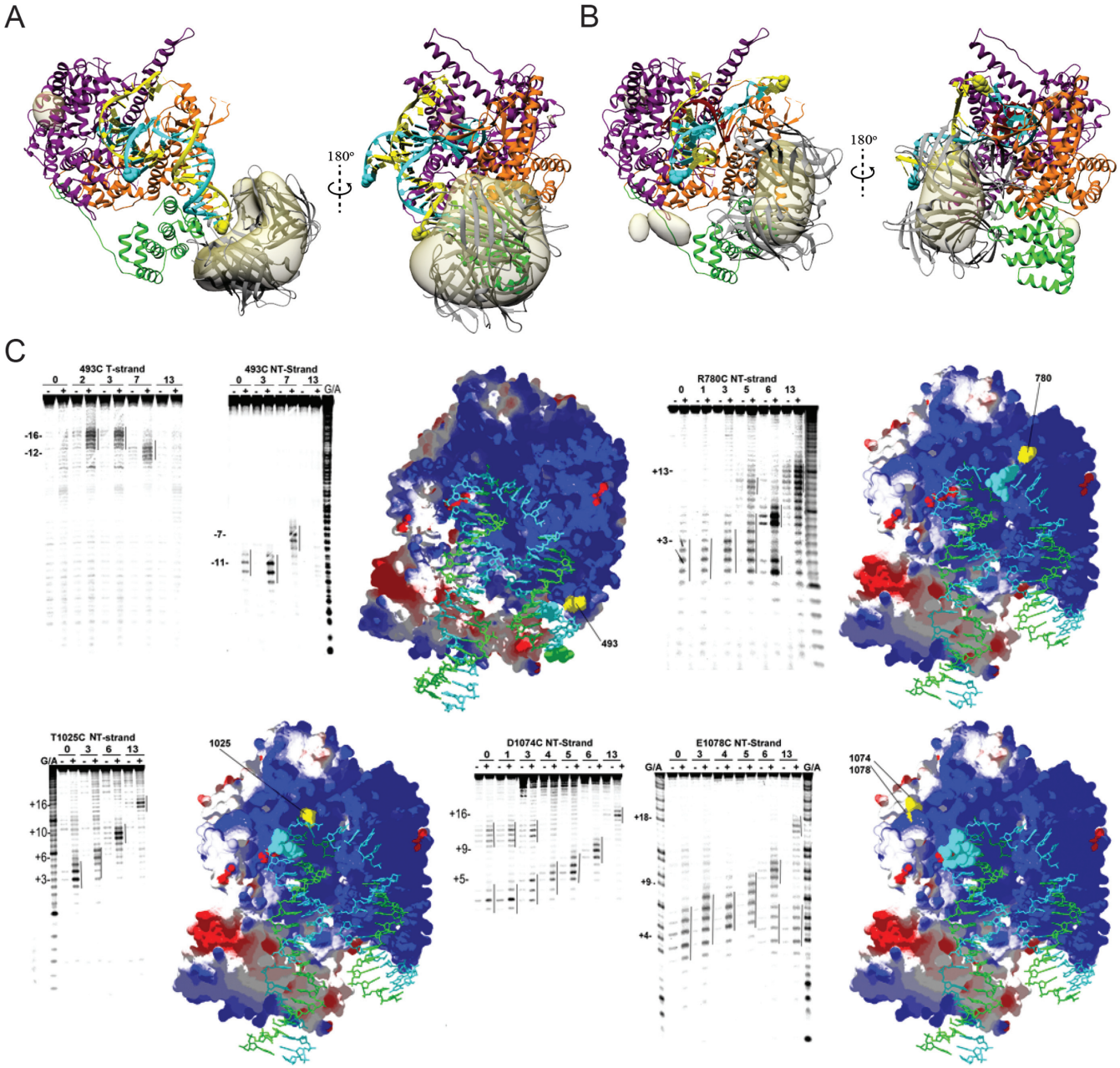

Figure 6. Displacement of the upstream end of DNA during the IC-EC transition. (**A**) Difference map (gray volume) generated by subtracting the IC from the upstream streptavidin IC with the atomic structure of streptavidin (gray) placed on the large density difference. The docked atomic structure of human MtRNAPEC (PDB ID: 4BOC, DNA not shown) and the DNA of aligned T7RNAPIC (3E2E) are shown and labeled as in Figure 5. (**B**) As in (A) but the subtraction is between EC and 'upstream streptavidin EC'. (**C**) Cleavage patterns of Fe-BABE molecules conjugated to the mtRNAP suggest conformational differences between the N-terminal domains of the IC and EC. Each panel shows the cleavages on either the NT- or T-strands, as indicated, in reactions with mtRNAP conjugated with Fe-BABE at the indicated residue positions. 'G/A' = markers used to map the cleavage sites with respect to the +1 transcription start site; '−' and '+' refer, respectively, to absence or addition of ascrobate/peroxide to activate cleavage (low levels of cutting are seen even in the absence of ascorbate/peroxide). NTPs allowing RNA extension to 0–13 nt, as indicated, were added to the reactions. Each panel also shows the MtRNAP structure in surface representation with −, + and uncharged regions in red, blue, and white, respectively. The DNA is in stick representation with the T-strand in green and the NT-strand in cyan. The position of the residue(s) to which Fe-BABE was conjugated is labeled and highlighted in yellow, and the centers of the sites of cleavage by those conjugates are indicated by showing the corresponding DNA nucleotides in space-filling representation (T-strand cleavage by conjugates at residues 780, 1025, 1074 and 1078 is not shown as it was very low, likely reflecting the fact that the proximal part of the T-strand is buried in the template binding cleft and inaccessible).

Table 1. Apparent K_{ATP} values for initiation from 14 s bubble or duplex promoter templates (values in μM and +/− S.E. for $n = 4$–5) and in either the absence of MTF1 (bubble templates only) or in the presence of WT MTF1 or MTFΔCterm

Bubble_NoMTF1	Bubble + MTF1	Bubble + MTF1ΔCterm	Duplex + MTF1	Duplex + MTF1ΔCterm	
110 ± 8.0	167 ± 19	197 ± 43	66 ± 8.9	579 ± 70	Dinucleotide
24 ± 4.0	78 ± 17	107 ± 27	52 ± 15	420 ± 70	Total
29 ± 4.0	44 ± 7.1	31 ± 11	43 ± 8.7	151 ± 17	Runoff

Values were determined by measuring the rate of dinucleotide synthesis in reactions with ATP only, or the rates of incorporation of NTPs into all transcripts ('Total') or only runoff transcript in reactions with all four NTPs (three NTPs at constant concentration and ATP varied). Deletion of the MTF1 C-terminus is seen to markedly increase K_{ATP} for initiation on duplex, but not bubble, templates.

DISCUSSION

Pol A class polymerases are characterized by conformational changes during their reaction cycles that involve opening and closing of the central template binding cleft around which these enzymes are organized. Rotation of the fingers subdomain toward the cleft accompanies binding of NTP or dNTP, while rotation of the fingers away from the cleft, causing it to become more open, occurs upon pyrophosphate release at the end of the nucleotide addition cycle (6–8,34–36). In addition to this transition, which is common to all pol A class enzymes, individual members of this family display distinct conformational changes, often involving distinct domains N-terminal to the common polymerase domain. In T7 RNAP, e.g. rotation of the NTD away from the polymerase domain progressively enlarges the template binding cleft to accommodate the growing RNA:DNA hybrid as the RNA is extended during initial transcription (37). A subsequent, large-scale conformational change in the NTD occurs upon transition to elongation, and ruptures promoter:RNAP interactions to allow promoter release and movement down the template DNA (7,34,36).

Human MtRNAP, in the absence of DNA or transcription factors, crystallized in a 'clenched' conformation that is more closed than any of the conformational states observed in the homologous T7 RNAP enzyme (23). Given the conformational malleability of these proteins, it is important to validate the physiological significance of the conformations observed in crystal structures because these conformations can be influenced by packing interactions or extreme crystallization solution conditions. Our EM data indicate that, under near-physiological solution environments, yeast MtRNAP assumes a tightly closed conformation similar to the clenched human MtRNAP state. The clenched conformation therefore appears to be a physiologically relevant state. Interestingly, the upstream ends of the DNAs seem to be similarly positioned in the characterized yeast quasi-IC and T7RNAP IC with 0 or 3 nts long RNA. This could mean that upon binding to MtRNAP, bubble or even duplex promoter DNAs assume a topology similar to the DNAs in the T7RNAP early ICs with 3-nt long RNAs.

However, as revealed by streptavidin labeling, the upstream end of the promoter in the quasi-IC is positioned far from the AT-rich recognition loop in the NTD of the mtRNAP, and is therefore less bent than the DNA in the IC. The latter interactions may be required to induce the sharp bending required for promoter opening. This could also explain why yeast MtRNAP alone is capable of starting transcription from bubble promoters, but not from duplex ones. Additionally, yeast MtRNAP alone binds relatively weakly to DNA and with relatively poor sequence specificity. MTF1 increases the stability and sequence specificity of the initiation complex (27,28). It is possible that, in the absence of MTF1, MtRNAP assumes a clenched conformation that associates weakly and non-specifically with DNA so that it can efficiently scan DNA for promoter sequences (Figure 7, quasi-IC). Encounter with a promoter could transiently slow this scanning to allow MTF1 binding, inducing the isomerization to the open state coupled with an increase of the DNA bending in the complex, as revealed by the different positions of streptavidin in this study, and consistent with previously reported differential bending of promoter DNA by yeast MtRNAP alone versus the yeast MtRNAP:MTF1 complex (28). Our EM data reveal how the MtRNAP and the MTF1 engage to form a functional IC, indicating that the upstream end of the DNA is brought into close proximity with the AT rich recognition loop of the NTD, which, together with MTF1, form a specific binding site for the upstream (−4 to −9 bp) promoter sequence (Figure 7, IC). As is also seen in T7RNAP, sequence specific binding of the promoter would therefore involve the NTD(s) and the promoter recognition loop (12,26), but would also involve MTF1, which generates promoter specificity through the conformational changes it induces in the polymerase and possibly also by making direct, sequence-specific interactions with the promoter. The sharp bending of the promoter in the IC complex would bring the DNA closer to the AT rich recognition loop, which would have a stabilizing effect on the MtRNAP:MTF1:DNA complex and would help drive promoter melting (28), as would interactions between MTF1 and the unwound NT strand (38), and between the MTF1 C-terminal tail and the melted regions of the promoter (39).

Published data do not clearly define the interaction between MtRNAP and MTF1. Deletions of the N-terminal and the C-terminal regions of MTF1 resulted in the absence or decreased yield of IC (40), suggesting the involvement of multiple regions in the MtRNAP:MTF1 interaction. Genetic screening has led to the identification of point mutations that cause loss or drastic decrease in mitochondrial transcription. These mutants are distributed in three clusters: region 1 (Y42C, H44P and L53H), region 2 (V135A, L154T and K157E) and region 3 (S218R, I221K and D225G). Mapping of these regions on the X-ray structure of MTF1 has revealed that they are not only facing different surfaces, but also that several of them are located in the interior of the protein (Supplementary Figure S7A–

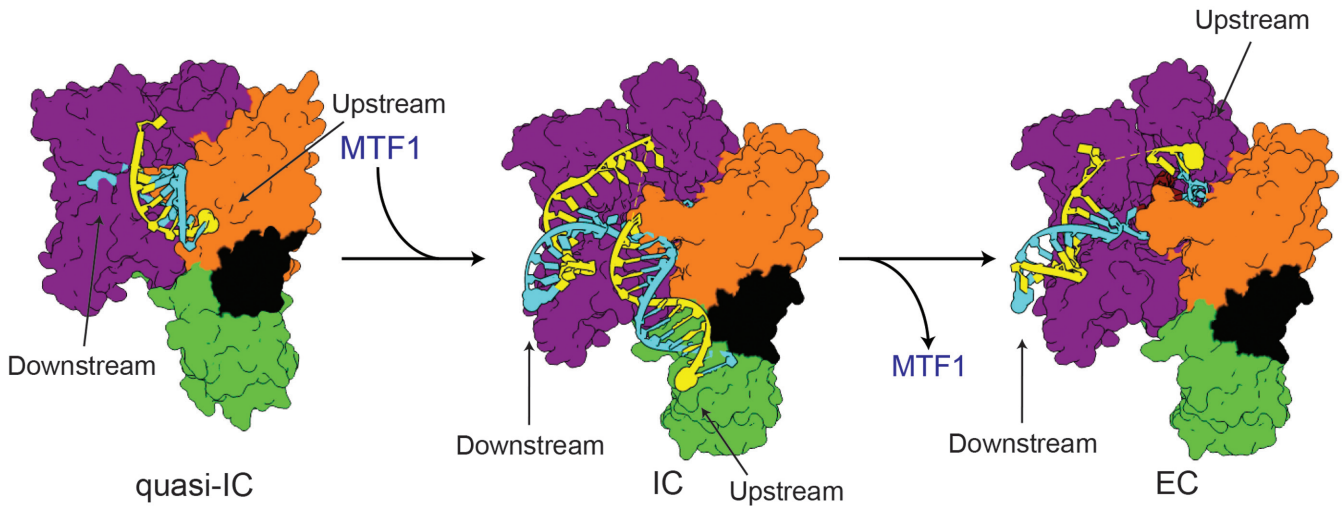

Figure 7. Modeling the transition from quasi IC to EC. The C-terminal-catalytic domain, the NTD, AT-rich recognition loop (residues 450–470) and the N-terminal extension and are represented by contours in purple (magenta), orange, black and green, respectively. The template and non-template DNA strands are colored yellow and cyan, respectively. The quasi-IC is characterized by a narrow template binding cleft and DNA binding that is not highly sequence specific. Binding of MTF1 to the quasi-IC (not shown in the cartoon) induces opening of the template binding cleft by rotation of the fingers and palm domains. The isomerization to the open state is coupled with additional bending of the upstream end of DNA, which is brought close to the NTD and the AT-rich recognition loop, which together with MTF1, form a sequence-specific binding site for the upstream regions of the promoter. Upon transition to elongation and dissociation of MTF1, the template binding cleft remains open with N-terminal regions not undergoing an extensive remodeling, as seen in T7RNAP, while the upstream end of DNA moves away from the NTD and the AT-rich recognition loop.

C), implying that they affect the structural integrity of the MTF1 rather than binding to MtRNAP (25). One of the proposed models (39) takes into account only those mutations that are in surface exposed residues: H44P of region 1, K157E of region 2 and all the amino acids of region 3, thus defining the interface where these residues are positioned as MTF1′s surface involved in interaction with MtRNAP. However, mutations R178A/K179A and H187A/R189A, which are located in the basic cleft at the interface of NH2 and COOH terminal subdomains, were previously shown to inactivate transcription on linear but not supercoiled DNA promoters (41), but are not accommodated in this model. A low-resolution structure of the human mtRNAP IC generated by EM and image processing has been recently reported (42) which reveals a completely different position for the transcription factors than that observed in this work for MTF1. However, we believe that the mentioned work suffers from certain problems, among others the low number of particles used in the study and the absence of any experimental evidence regarding the location of the individual components which could have led to an incorrect organization of the IC (Supplementary Figure S7D and E). Our structural study provides a more precise and in-depth insight into the organization of IC state, complementing and allowing the evaluation of information gathered by biochemical and biophysical approaches (25,39,43,44). Thus, our EM study shows for the first time how these two proteins interact and, furthermore, excludes these hypothetical models, as the region 3 and the remaining superficially exposed amino acids of region 1 and 2 are placed at the opposite, outer face of MTF1. Additionally, our data places the positively charged cleft of MTF1 toward the MtRNAP and the DNA (Supplementary Figure S7B and C).

Transcription initiation requires the formation of stable and specific interactions between the RNAP and the promoter, which lead to its bending and tension accumulation. This tension is released through the promoter melting and formation of the upstream edge of transcription bubble, generally in the AT rich regions of the promoters. In T7 RNAP three structural elements-(1) the AT rich recognition loop (residues 93–101); (2) the specificity loop (residues 739–770); and (3) the intercalating β- hairpin including Val237 (residues 230–245) are responsible for the promoter recognition, binding and melting. RNAPs remains bound to their promoters as the RNA is extended to a length that triggers promoter release and transition to elongation. The T7RNAP IC to EC transition involves large structural rearrangement of the entire NTD and specificity loop, resulting in the loss of all contacts with the promoter and the formation of the RNA exit channel (34). The C-terminal, catalytic domain undergoes fewer conformational changes. Our EM reconstructions of MtRNAP IC and EC reveal that, consistent with what has been previously observed (9,24), that the N-terminal part of protein, unlike in T7RNAP, does not change conformation during the IC–EC transition (Figure 7, EC). Unlike what is seen with T7RNAP, promoter release and transition to elongation do not depend on conformational changes in the promoter binding elements of the mtRNAP. Instead, MtRNAPs recruit dissociable transcription factor(s) which, in the initiation phase of transcription drive a transition from a clenched to an open conformation in the mtRNAP, and allow for promoter recognition, melting and stabilization of the IC. Subsequently, these factors become displaced and allow promoter release once the RNA reaches a length sufficient for formation of a stable MtRNAP:DNA:RNA complex.

SUPPLEMENTARY DATA

Supplementary Data are available at NAR Online.

ACCESSION NUMBERS

PDB IDs: 3SPA, 4BOC, 1I4W, 1N43, 3E2E and 1QLN.

FUNDING

Spanish Ministry of Science and Innovation [BFU2010-15703, BFU2013-44202 to J.M.V.]; National Institutes of Health [GM0502522 to R.S.]. La Caixa foundation fellowship [to S.D.].Funding for open access charge: Spanish Ministry of Science and Innovation [BFU2013-44202] [to J.M.V.].
Conflict of interest statement. None declared.

REFERENCES

1. Cermakian,N., Ikeda,T.M., Cedergren,R. and Gray,M.W. (1996) Sequences homologous to yeast mitochondrial and bacteriophage T3 and T7 RNA polymerases are widespread throughout the eukaryotic lineage. *Nucleic Acids Res.*, **24**, 648–654.
2. Cermakian,N., Ikeda,T.M., Miramontes,P., Lang,B.F., Gray,M.W. and Cedergren,R. (1997) On the evolution of the single-subunit RNA polymerases. *J. Mol. Evol.*, **45**, 671–681.
3. Sousa,R. (1996) Structural and mechanistic relationships between nucleic acid polymerases. *Trends Biochem. Sci.*, **21**, 186–190.
4. Lee,D.Y. and Clayton,D.A. (1998) Initiation of mitochondrial DNA replication by transcription and R-loop processing. *J. Biol. Chem.*, **273**, 30614–30621.
5. Masters,B.S., Stohl,L.L. and Clayton,D.A. (1987) Yeast mitochondrial RNA polymerase is homologous to those encoded by bacteriophages T3 and T7. *Cell*, **51**, 89–99.
6. Beese,L.S., Derbyshire,V. and Steitz,T.A. (1993) Structure of DNA polymerase I Klenow fragment bound to duplex DNA. *Science*, **260**, 352–355.
7. Yin,Y.W. and Steitz,T.A. (2004) The structural mechanism of translocation and helicase activity in T7 RNA polymerase. *Cell*, **116**, 393–404.
8. Cheetham,G.M. and Steitz,T.A. (2000) Insights into transcription: structure and function of single-subunit DNA-dependent RNA polymerases. *Curr. Opin. Struct. Biol.*, **10**, 117–123.
9. Ringel,R., Sologub,M., Morozov,Y.I., Litonin,D., Cramer,P. and Temiakov,D. (2011) Structure of human mitochondrial RNA polymerase. *Nature*, **478**, 269–273.
10. Matsunaga,M. and Jaehning,J.A. (2004) Intrinsic promoter recognition by a 'core' RNA polymerase. *J. Biol. Chem.*, **279**, 44239–44242.
11. Mangus,D.A., Jang,S.H. and Jaehning,J.A. (1994) Release of the yeast mitochondrial RNA polymerase specificity factor from transcription complexes. *J. Biol. Chem.*, **269**, 26568–26574.
12. Nayak,D., Guo,Q. and Sousa,R. (2009) A promoter recognition mechanism common to yeast mitochondrial and phage t7 RNA polymerases. *J. Biol. Chem.*, **284**, 13641–13647.
13. Mukherjee,S., Brieba,L.G. and Sousa,R. (2002) Structural transitions mediating transcription initiation by T7 RNA polymerase. *Cell*, **110**, 81–91.
14. Mukherjee,S. and Sousa,R. (2003) Use of site-specifically tethered chemical nucleases to study macromolecular reactions. *Biol. Proced. Online*, **5**, 78–89.
15. Guo,Q. and Sousa,R. (2005) Multiple roles for the T7 promoter nontemplate strand during transcription initiation and polymerase release. *J. Biol. Chem.*, **280**, 3474–3482.
16. Mindell,J.A. and Grigorieff,N. (2003) Accurate determination of local defocus and specimen tilt in electron microscopy. *J. Struct. Biol.*, **142**, 334–347.
17. Marabini,R., Masegosa,I.M., San Martin,M.C., Marco,S., Fernandez,J.J., de la Fraga,L.G., Vaquerizo,C. and Carazo,J.M. (1996) Xmipp: an image processing package for electron microscopy. *J. Struct. Biol.*, **116**, 237–240.
18. Scheres,S.H. (2010) Classification of structural heterogeneity by maximum-likelihood methods. *Methods Enzymol.*, **482**, 295–320.
19. Sorzano,C.O., Bilbao-Castro,J.R., Shkolnisky,Y., Alcorlo,M., Melero,R., Caffarena-Fernandez,G., Li,M., Xu,G., Marabini,R. and Carazo,J.M. (2010) A clustering approach to multireference alignment of single-particle projections in electron microscopy. *J. Struct. Biol.*, **171**, 197–206.
20. Ludtke,S.J., Baldwin,P.R. and Chiu,W. (1999) EMAN: semiautomated software for high-resolution single-particle reconstructions. *J. Struct. Biol.*, **128**, 82–97.
21. Pettersen,E.F., Goddard,T.D., Huang,C.C., Couch,G.S., Greenblatt,D.M., Meng,E.C. and Ferrin,T.E. (2004) UCSF Chimera–a visualization system for exploratory research and analysis. *J. Comput. Chem.*, **25**, 1605–1612.
22. Jang,S.H. and Jaehning,J.A. (1991) The yeast mitochondrial RNA polymerase specificity factor, MTF1, is similar to bacterial sigma factors. *J. Biol. Chem.*, **266**, 22671–22677.
23. Ringel,R., Sologub,M., Morozov,Y.I., Litonin,D., Cramer,P. and Temiakov,D. Structure of human mitochondrial RNA polymerase. *Nature*, **478**, 269–273.
24. Schwinghammer,K., Cheung,A.C., Morozov,Y.I., Agaronyan,K., Temiakov,D. and Cramer,P. (2013) Structure of human mitochondrial RNA polymerase elongation complex. *Nat. Struct. Mol. Biol.*, **20**, 1298–1303.
25. Schubot,F.D., Chen,C.J., Rose,J.P., Dailey,T.A., Dailey,H.A. and Wang,B.C. (2001) Crystal structure of the transcription factor sc-mtTFB offers insights into mitochondrial transcription. *Protein Sci.* , **10**, 1980–1988.
26. Cheetham,G.M., Jeruzalmi,D. and Steitz,T.A. (1999) Structural basis for initiation of transcription from an RNA polymerase-promoter complex. *Nature*, **399**, 80–83.
27. Velazquez,G., Guo,Q., Wang,L., Brieba,L.G. and Sousa,R. (2012) Conservation of promoter melting mechanisms in divergent regions of the single-subunit RNA polymerases. *Biochemistry*, **51**, 3901–3910.
28. Tang,G.Q., Deshpande,A.P. and Patel,S.S. (2011) Transcription factor-dependent DNA bending governs promoter recognition by the mitochondrial RNA polymerase. *J. Biol. Chem.*, **286**, 38805–38813.
29. Steitz,T.A. (2009) The structural changes of T7 RNA polymerase from transcription initiation to elongation. *Curr. Opin. Struct. Biol.*, **19**, 683–690.
30. Cheetham,G.M. and Steitz,T.A. (1999) Structure of a transcribing T7 RNA polymerase initiation complex. *Science*, **286**, 2305–2309.
31. Greiner,D.P., Miyake,R., Moran,J.K., Jones,A.D., Negishi,T., Ishihama,A. and Meares,C.F. (1997) Synthesis of the protein cutting reagent iron (S)-1-(p-bromoacetamidobenzyl)ethylenediaminetetraacetate and conjugation to cysteine side chains. *Bioconjug. Chem.*, **8**, 44–48.
32. Kravchenko,J.E., Rogozin,I.B., Koonin,E.V. and Chumakov,P.M. (2005) Transcription of mammalian messenger RNAs by a nuclear RNA polymerase of mitochondrial origin. *Nature*, **436**, 735–739.
33. Paratkar,S., Deshpande,A.P., Tang,G.Q. and Patel,S.S. (2011) The N-terminal domain of the yeast mitochondrial RNA polymerase regulates multiple steps of transcription. *J. Biol. Chem.*, **286**, 16109–16120.
34. Yin,Y.W. and Steitz,T.A. (2002) Structural basis for the transition from initiation to elongation transcription in T7 RNA polymerase. *Science*, **298**, 1387–1395.
35. Temiakov,D., Patlan,V., Anikin,M., McAllister,W.T., Yokoyama,S. and Vassylyev,D.G. (2004) Structural basis for substrate selection by t7 RNA polymerase. *Cell*, **116**, 381–391.
36. Tahirov,T.H., Temiakov,D., Anikin,M., Patlan,V., McAllister,W.T., Vassylyev,D.G. and Yokoyama,S. (2002) Structure of a T7 RNA polymerase elongation complex at 2.9 A resolution. *Nature*, **420**, 43–50.
37. Durniak,K.J., Bailey,S. and Steitz,T.A. (2008) The structure of a transcribing T7 RNA polymerase in transition from initiation to elongation. *Science*, **322**, 553–557.
38. Paratkar,S. and Patel,S.S. (2010) Mitochondrial transcription factor Mtf1 traps the unwound non-template strand to facilitate open complex formation. *J. Biol. Chem.*, **285**, 3949–3956.
39. Savkina,M., Temiakov,D., McAllister,W.T. and Anikin,M. (2010) Multiple functions of yeast mitochondrial transcription factor Mtf1p during initiation. *J. Biol. Chem.*, **285**, 3957–3964.

40. Cliften,P.F., Park,J.Y., Davis,B.P., Jang,S.H. and Jaehning,J.A. (1997) Identification of three regions essential for interaction between a sigma-like factor and core RNA polymerase. *Genes Dev.*, **11**, 2897–2909.
41. Shadel,G.S. and Clayton,D.A. (1995) A Saccharomyces cerevisiae mitochondrial transcription factor, sc-mtTFB, shares features with sigma factors but is functionally distinct. *Mol. Cell. Biol.*, **15**, 2101–2108.
42. Yakubovskaya,E., Guja,K.E., Eng,E.T., Choi,W.S., Mejia,E., Beglov,D., Lukin,M., Kozakov,D. and Garcia-Diaz,M. (2014) Organization of the human mitochondrial transcription initiation complex. *Nucleic Acids Res.*, **42**, 4100–4112.
43. Bandwar,R.P., Ma,N., Emanuel,S.A., Anikin,M., Vassylyev,D.G., Patel,S.S. and McAllister,W.T. (2007) The transition to an elongation complex by T7 RNA polymerase is a multistep process. *J. Biol. Chem.*, **282**, 22879–22886.
44. Tang,G.Q., Paratkar,S. and Patel,S.S. (2009) Fluorescence mapping of the open complex of yeast mitochondrial RNA polymerase. *J. Biol. Chem.*, **284**, 5514–5522.